Vol. 552: 93–113, 2016
doi: 10.3354/meps11742

MARINE ECOLOGY PROGRESS SERIES
Mar Ecol Prog Ser

Published June 23

Enhanced CO_2 concentrations change the structure of Antarctic marine microbial communities

Andrew T. Davidson[1,2,3,*], John McKinlay[1], Karen Westwood[1,2,3], Paul G. Thomson[4], Rick van den Enden[1], Miguel de Salas[5], Simon Wright[1,2,3], Robert Johnson[3], Kate Berry[6]

[1]Department of the Environment and Water Resources, Australian Antarctic Division, Channel Highway, Kingston, Tasmania 7050, Australia

[2]Antarctic Climate and Ecosystems Cooperative Research Centre (ACE CRC), University of Tasmania, Private Bag 80, Hobart, Tasmania 7001, Australia

[3]Institute of Marine and Antarctic Studies (IMAS), University of Tasmania, Private Bag 129, Hobart, Tasmania 7001, Australia

[4]School of Environmental Systems Engineering and The UWA Oceans Institute, The University of Western Australia, Mailstop M470, 35 Stirling Highway, Crawley, Western Australia 6009, Australia

[5]Tasmanian Herbarium, Tasmanian Museum and Art Gallery, College Rd., Sandy Bay, Tasmania 7005, Australia

[6]CSIRO Marine and Atmospheric Research (CMAR), CSIRO Marine and Atmospheric Research Laboratories, Castray Esplanade, Hobart, Tasmania 7000, Australia

ABSTRACT: The impacts of anthropogenic enhancement of the partial pressure of carbon dioxide (pCO_2) on marine organisms remain unclear, especially in Antarctic waters, which are predicted to be amongst the earliest and most severely affected by the consequent changes in ocean chemistry. Marine microbes are the base of the Antarctic food chain, and the nature of their response to elevated pCO_2 is important as they are key determinants of the biogeochemical cycles that affect global climate. We studied the response of a natural community of Antarctic marine microbes from near-shore waters off Davis Station, Antarctica, to pCO_2 ranging from the concentration in the water column at the time the experiment began (ambient, 84 µatm) to that predicted by the year 2300 (2423 µatm) using 6 gas-tight, environmentally controlled tanks (minicosms; 650 l) to which CO_2-saturated seawater was added. The microbial community showed little difference between 84 and 643 µatm CO_2 (0.2 to 1.7 times present), indicating that they can tolerate the large seasonal range in pCO_2 in Antarctic coastal waters. Concentrations ≥1281 µatm reduced the accumulation rate of chlorophyll and particulate carbon, changed the microbial community, and enhanced the relative abundance of small phytoplankton. If our results are indicative of the future responses of Antarctic marine microbes, elevated CO_2 could profoundly affect the structure and function of the Antarctic food web by reducing the availability of food for higher trophic levels and decreasing the efficiency of the biological pump.

KEY WORDS: Ocean acidification · Phytoplankton · Microzooplankton · Bacteria · Community structure · Abundance · Size · Biomass

INTRODUCTION

Marine microbes are the foundation of the Southern Ocean food web, but little is known about their sensitivity to elevated partial pressure of carbon dioxide (pCO_2), the implications for the structure and function of microbial communities, or the feedbacks to global climate. Antarctic waters are amongst the most vulnerable of the world's oceans to anthropogenic enhancement of CO_2 concentrations. Southern Ocean CO_2 concentrations are enhanced by the high solubility of CO_2 in cold water and the upwelling of

*Corresponding author: andrew.davidson@aad.gov.au

CO_2-rich waters at the Antarctic Slope Front. In addition, the extreme seasonality of Southern Ocean production changes the ratio between CO_2 draw-down by photosynthesis and its release by respiration (Delille 2004, Joint et al. 2011). As a result, pCO_2 falls as low as 100 µatm during intense summer phytoplankton blooms but can reach 450 µatm in autumn and winter when light is limited or absent and air–sea gas exchange is limited by sea ice cover (Gibson & Trull 1999, McNeil et al. 2011, Roden et al. 2013). This range is almost 6 times the current anthropogenic enhancement of pCO_2 and amongst the largest for any oceanic region (Takahashi et al. 2002). Anthropogenic increases in CO_2 concentration are superimposed on these large natural variations, exposing the organisms that inhabit the Southern Ocean to extremely variable, but often high, CO_2 concentrations. Evidence from the west coast of the USA has shown that even organisms that tolerate a wide natural range in pCO_2 can suffer a dramatic decline in survival if naturally high CO_2 concentrations are anthropogenically enhanced (Feely et al. 2008, Barton et al. 2012).

CO_2-induced changes to the microbial loop could have widespread consequences. Some of the organic matter produced by phytoplankton fuels the food web and supports the wealth of life for which Antarctica is renowned, or sinks to the deep ocean and reduces the accumulation of CO_2 in the atmosphere (the biological pump) (e.g. Ducklow et al. 2001). However, the large biomass and rapid metabolism of marine microbes mean that much of the carbon sequestered by phytoplankton can be grazed by protozoa, remineralised by heterotrophic bacteria, or released as dissolved organic carbon by viral lysis (e.g. Froneman & Perissinotto 1996, Azam 1998, Pomeroy et al. 2007, Miki & Jacquet 2008). Thus, CO_2-induced changes in the structure and function of Antarctic microbial communities could alter trophodynamics and biogeochemistry in the Southern Ocean.

Most studies of enhanced pCO_2 on marine phytoplankton have determined the effects on single species or trophic levels and have been conducted using organisms from temperate to tropical waters, showing effects that range from inhibition to promotion (e.g. Hinga 2002, Tortell et al. 2002, Rost et al. 2003, 2008, Hendriks et al. 2010, Engel et al. 2013, Trimborn et al. 2013, Gattuso et al. 2015). The few studies from polar waters commonly find that enhanced CO_2 changes the phytoplankton species composition and favours large diatoms (Engel et al. 2008, Tortell et al. 2008, Feng et al. 2010). However, other studies have shown that elevated CO_2 concentrations promote the growth of pico- and/or nanoplankton (e.g. Hare et al. 2007, Brussaard et al. 2013). Clearly, much remains to be learned about the factors dictating the effects of CO_2 on marine phytoplankton.

Less still is known of the effects of enhanced CO_2 on other members of the microbial loop. A mesocosm incubation in Arctic waters found little effect of elevated pCO_2 on microzooplankton grazing (Suffrian et al. 2008). Other studies show CO_2-induced changes in the phytoplankton community composition can indirectly affect microzooplankton abundance and/or grazing rates (Rose et al. 2009, Brussaard et al. 2013). Similarly, the little information available suggests viruses are not directly affected by CO_2 concentrations from 350 to 1050 µatm but will be indirectly influenced by impacts on host organisms (Larsen et al. 2008, Danovaro et al. 2011). Such changes may alter the proportion of photoassimilated carbon diverted into the dissolved carbon pool (Brussaard et al. 2013). Changes in pCO_2 have reportedly had little effect on the composition and abundance of heterotrophic bacteria (Grossart et al. 2006, Joint et al. 2011 and references therein), but evidence of its effects on bacterial ectoenzyme activity differ among studies (Piontek et al. 2010, Yamada & Suzumura 2010, Endres et al. 2014). Together these studies suggest that community-level interactions are likely to play a major role in determining the nature and magnitude of changes in the microbial loop as a result of increasing CO_2. Yet little is known about the effects of elevated pCO_2 on these communities (Gattuso et al. 2015), despite this knowledge being vital to predicting CO_2-induced changes on carbon fixation, flux and fate in the ocean.

Studies using single species or trophic levels are poorly suited to predicting the effects of environmental change on natural ecosystems as they do not incorporate changes in competitive and trophic-level interactions (Davidson 2006). To determine the effects of elevated pCO_2 on the structure and function of the microbial loop in Antarctic waters, we conducted a minicosm experiment using a natural community of Antarctic marine microbes from Davis Station, Antarctica. This was designed to answer the following questions:

(1) Are Antarctic marine microbial communities affected by enhanced concentrations of CO_2? If so, what are these changes and what is the threshold CO_2 concentration for a response?

(2) How rapidly can enhanced CO_2 change the structure of a marine microbial community?

(3) What are the mechanisms by which CO_2 may change the microbial community?

MATERIALS AND METHODS

Since communities naturally experience a wide range in pCO_2, and we had no prior data on their sensitivity to enhanced CO_2 conditions, our experiments encompassed CO_2 concentrations ranging from 84 to 2423 µatm, representing concentrations from ambient to post-2300 AD conditions (Caldeira & Wickett 2003). We were constrained to 6 minicosms, which we ran as an unreplicated 6-level dose-response experiment to best determine a threshold response, rather than replicating fewer treatments that may have missed the critical threshold. Furthermore, since we also had no data on the timing of any response, we did not include an acclimation period during which the physiology of cells or the composition of the community was allowed to adjust to the change in CO_2 environment. Instead we started sampling immediately after adjustment of the pCO_2 in the minicosms.

Minicosm operation

Microbial assemblages were incubated in six 650 l polythene incubation tanks (minicosms) that were housed in a temperature-controlled shipping container. All minicosms were cleaned with detergent (Decon 90), sprayed with 10% vol:vol AR grade HCl and thoroughly rinsed with MilliQ water. Finally, tanks were rinsed (filled and drained) with ambient seawater before being filled with the microbial community that was incubated.

Minicosms were filled with natural microbial assemblage obtained from near-shore waters off Davis Station, Antarctica (68° 35′ S, 77° 58′ E) on 30 December 2008, 3 wk after the disappearance of land-fast sea ice. Seawater was pumped to the minicosms from 60 m offshore at 2 m depth using a Teflon double diaphragm pump fitted to Teflon-lined hosing that had 200 µm mesh over the intake to exclude metazooplankton. All 6 minicosms tanks were filled simultaneously to ensure they contained the same initial microbial community. The water temperature in each tank was measured to ± 0.01°C and maintained at ambient ± 0.1°C by cooling the shipping container, offset against warming of each tank's contents by two 300 W aquarium heaters (Fluval) that were connected to a predictive temperature-control program via Carel temperature controllers. The content of each minicosm was gently mixed with a high-density polyethylene shrouded auger (cleaned as above) rotating at 15 rpm and illuminated on a 19 h light:5 h dark cycle by two 150W HQI-TS metal halide lamps (Osram). With the exception of minor emission peaks at approximately 420, 540, 580, and 670 nm wavelength, the spectral emission of the lights was similar to solar radiation (www.osram.com.au/media/resource/hires/335357/powerstar-hqi-ts-excellence-70-w-and-150-w—the-latest-innovation-in-quartz-tec.pdf). Emission from the lamps was filtered with 1/4 CT blue filter (Arri), which attenuated wavelengths <500 nm by ~20% while those greater than 550 nm were attenuated ~40%. This gave an average light intensity in the minicosm tanks of 200 µmol m^{-2} s^{-1}, which equated to ~50% of the daily noon-time clear-sky irradiance at 5 m depth at Davis Station and provided ~21% of the average daily downwelling dose of photosynthetically active radiation (PAR) at this site around the summer solstice (Thomson et al. 2008). The minicosm tanks were covered by acrylic lids and were gas tight except during periods of pCO_2 manipulation and on sampling days when sample removal required an increase in the headspace volume.

All measurements were obtained from each minicosm over 10 d. Carbonate chemistry in each minicosm was measured at the start of the experiment and adjusted to achieve the desired experimental pCO_2 (see next subsection). These measurements and adjustments were performed daily to maintain the target pCO_2 in each minicosm. Bulk parameters (nutrients, chl *a*, particulate organic carbon (POC) and carbon to nitrogen ratio) were measured every 2 d and are presented over the entire 10 d of the experiment.

Measurements of the microbial community were also obtained every 2 d over the 10 d; however, we restricted presentation of these results to include only the first 8 d of the experiment during which time nutrients were sufficient to sustain growth of phytoplankton in all CO_2 treatments. This avoided nutrient limitation in some tanks confound our ability to detect CO_2-induced changes in the microbial community (see Fig. 2). As all tanks were simultaneously filled with the same seawater, only 3 tanks were randomly chosen for the initial sampling at time 0. All tanks were sampled every 2 d thereafter.

Samples for carbonate chemistry were gently collected using a Teflon line located at the bottom of an acid-cleaned and MilliQ-rinsed 200 ml bottle. The bottle was rinsed with tank contents, then filled to overflowing and capped with a convex lid to exclude air. For other samples, an acid-cleaned and MilliQ-rinsed 20 l black polythene drum was filled from each minicosm at 08:30 h local time ± 30 min, transferred to the laboratory, retained at 0°C, and samples were obtained to determine microbial community composition

and abundance (flow cytometry, light and electron microscopy, pigments); POC; and macronutrient concentrations, namely nitrate + nitrite (NO_x), soluble reactive phosphorous (SRP) and molybdate-reactive silicate (silicate). The total volume of samples removed from each minicosm did not exceed 20% of its initial volume.

Water chemistry

Carbonate chemistry

Concentrations of CO_2 in the minicosm tanks were manipulated by adding CO_2-saturated seawater that had been 0.22 µm filtered, thereby conforming to the recommended best practice guidelines for manipulating CO_2 concentration in studies of ocean acidification (Gattuso et al. 2010, Schulz et al. 2013). CO_2 concentrations in the tanks averaged 84, 643, 1281, 1848, 1942 and 2423 µatm; equating to 0.2, 1.7, 3.3, 4.8, 5.0 and 6.3 times the global atmospheric pCO_2 (386 µatm) at the time the experiments were performed (http://co2now.org/). Logistic constraints, namely the size of the shipping container and the required volume of each minicosm, limited the number of incubation tanks to 6.

Measurements of temperature, salinity and atmospheric pressure that were necessary to estimate carbonate chemistry were determined using the thermometers in each minicosm tank (above), a WTW LF197 conductivity meter and observations by the Bureau of Meteorology at Davis Station, respectively.

Calculations of carbonate chemistry during our experiment were based on measurements of total alkalinity (TA) and pH. A Metrohm 809 Titrando and single 800 Dosino auto-titrator was used to determine TA by open cell potentiometric titration (SOP 3b, Dickson et al. 2007). The pH probe used to record the titration was calibrated to high accuracy buffers of pH 4.010 and 10.010 (Hanna). Our estimates of TA were within 0.7% of TA standards obtained from Andrew G. Dickson (University of California, pers. comm.), and this offset was used to correct the measured alkalinity in minicosm samples.

A Mettler Toledo Easy Seven meter was used to measure seawater pH (SOP 6a, Dickson et al. 2007). The Excel macro 'CO2SYS.BAS' (Lewis & Wallace 1998) was used to calculate pH of known TA and salinity (Dickson TA standards) that had been bubbled with nitrogen and pure CO_2 for ≥ 30 min. The pH meter was then manually calibrated to these samples at the calculated pH. The temperature of pH standards was measured using an NIST calibrated Guildline 9540, 3 decimal place platinum resistance thermometer and all pH measurements were performed in a closed vessel to avoid losses of aqueous CO_2.

Calculations of carbonate chemistry were further constrained by measurements of total CO_2 (TCO_2). A glass 250 ml bottle, containing 100 µl of a saturated solution of mercuric chloride, was gently filled with sample and the bottle tightly capped using a lid with a convex insert to exclude all air. The samples were retained at 4°C and returned to Australia for determination of TCO_2 at CSIRO Marine Laboratories, Hobart following the procedure in Dickson et al. (2007).

CO2SYS.BAS software was used to calculate the volume of CO_2-saturated seawater required to adjust each minicosm tank to the target CO_2 concentration. Coastal seawater was collected into an acid-cleaned black polythene drum (as above), gravity-filtered through a 0.2 µm pore size AcroPak 500 cartridge filter (Pall) into a 20 l acid-cleaned drum and bubbled with CO_2 gas (BOC, food grade) for 1 h until saturated (as determined by the pH meter). This CO_2-saturated water was added over ~2 h using medical saline infusion bags with intravenous drips to regulate flow rate (Baxter). Daily measurement and adjustment of carbonate chemistry in each tank (above) compensated for photosynthetic draw-down of CO_2 by phytoplankton.

Nutrients

Macronutrients were not added to the minicosms during the experiments; however, Fe-EDTA (5 nM final concentration) was added to each tank at the beginning of the experiment. This avoided iron-induced variation in microbial growth among tanks, as the tanks could not be rendered trace-metal clean. Nutrient samples were obtained every 2 d from each tank, filtered through Millex HA 0.45 cellulose ester filters (Millipore) and frozen at −20°C for later analysis. Concentrations of NO_x, SRP) and silicate were determined by Analytical Services Tasmania (AST), Department of Primary Industries, Parks, Water and Environment, Tasmanian Government using flow injection analysis in accordance with the APHA standard methods 4500-NO_3^- I, 4500-P G and 4500-SiO_2 F, respectively (Anonymous 2005). Briefly, NO_x concentrations were determine by reduction of nitrate to nitrite with copperised cadmium. The concentration of all nitrite was then measured by diazotization with sulfanilamide dihydrochloride, staining with N(1-napthyl) ethylenediamine dihydrochloride

(NED) and the absorbance of the sample measurement at 540 nm wavelength. SRP was quantified by complexing PO_4^{3-} with ammonium molybdate under acidic conditions, the complex reduced with stannous chloride and the absorbance measured at a wavelength of 880 nm. Concentrations of silicate were determined by complexing silicate with molybdate at ~pH 1.2, reducing the complex with stannous chloride, addition of oxalic acid to remove interference of phosphate complexes and measurement of the sample at a wavelength of 820 nm. Operational detection limits for NO_x, SRP and silicate were 0.14, 0.10 and 1.66 µM, respectively.

Microbial structure and abundance

Microscopy

Samples from each minicosm were analysed to determine the protistan identity, abundance and trophic status. Sub-samples of 960 ml were fixed with Lugol's iodine and the protists concentrated by sedimentation to ~100 ml. The samples were stored in the dark at 4 °C until counted (within 6 mo). The final volume of the concentrate was measured and, depending on cell density, sub-samples of 3 to 10 ml were settled for 2 d in 10 ml sedimentation cylinders (Hydro-Bios, Keil). Counts were performed over 20 randomly chosen quadrats (Whipple grids) at 400× magnification by inverted microscopy using Nomarski interference optics.

Determining the identity and trophic status of cryptic protistan taxa was aided by epifluorescent and scanning electron microscopy (SEM). Autotrophic protists were distinguished from heterotrophs by taxonomic identity, the presence of chloroplasts and chlorophyll autofluorescence. Samples of ~1 l were obtained from each of the minicosm tanks at the beginning and end of the incubations, concentrated to approximately 4 ml over a 47 mm, 0.8 µm polycarbonate filter (Poretics) and fixed by adding sufficient (~160 µl) 25% electron microscope-grade glutaraldehyde (ProSciTech) to obtain a 1% final concentration. A drop of cell concentrate (~0.03 ml) was immediately transferred to a microscope slide and examined at 400× magnification under Nomarski optics and blue epifluorescense (filter set 487909 with 450 to 490 nm exciter filter, 510 chromatic beam splitter and 520 nm barrier filter) using a Zeiss Axioscop inverted microscope. The presence of chlorophyll autofluorescence in a species indicated it was likely to be autotrophic (MacIsaac & Stockner 1993).

The remainder of the glutaraldehyde-fixed concentrate (see above) was refrigerated at 4 °C, transported to Australia and prepared for SEM in Australia using a modified polylysine technique (Marchant & Thomas 1983). Samples were post-fixed with OsO_4 vapour for 30 min, sedimented onto polylysine-coated coverslips, dehydrated over a graded ethanol series and immersed in 100% dry acetone before being critically point dried in a Balzers Union 020 CPD using liquid CO_2. The coverslips were then mounted on 12.5 mm diameter aluminium stubs, sputter-coated in a Cressington 208HRD coater with 7 nm of platinum/paladium (Pt/Pd) and imaged in a JEOL JSM6701F Field Emission Scanning Electron Microscope (FESEM).

The abundances of the 116 different protistan taxa/groups >20 µm in size were determined from microscopic cell counts of sedimented samples, while the abundance of small microbes (nano- and picoplankton) was determined by flow cytometry. The total number of cells >20 µm in size were counted in the 20 quadrats for each sample increased from approximately 200 at the beginning of the experiments to approximately 1400 on Day 8. Cells were identified to the lowest possible taxonomic level, based on descriptions in Tomas (1997) and Scott & Marchant (2005). Microscope counts of the 4 dominant protistan taxa in our study had low variance among quadrats. Despite the high number of total cells counted, all other taxa were infrequent, had high quadrat-level variance for individual samples or had implausibly high variability among times in a single treatment. These taxa were pooled into 3 functional groups of protists, namely centric diatoms, other phytoplankton taxa (pennate diatoms and infrequent dinoflagellates) or heterotrophs (dinoflagellates and infrequent ciliates). A further 6 functional groups of nano- and picoplankton were resolved by flow cytometry (see next section).

Where possible, the average dimensions of 50 cells of each of the 116 taxa/groups were measured using an eyepiece micrometer. For rarer species, all cells observed were measured and these measurements were supplemented with values from the literature. The cell volume was then calculated and converted to equivalent spherical diameter (ESD).

Flow cytometry

Flow cytometric analyses were performed using Becton Dickinson flow cytometers fitted with 488 nm lasers. The abundance of nano- and pico-sized protists was determined using a FACScan, while bacter-

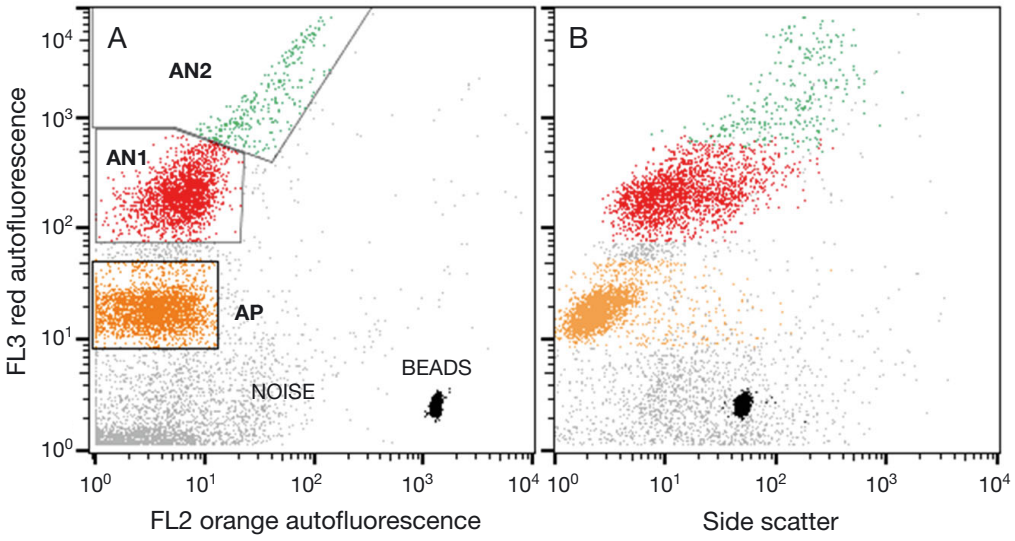

Fig. 1. Pico- and nanophytoplankton populations identified by flow cytometry. (A) Populations of autotrophic picoplankton (AP) and autotrophic nanoplankton (AN1 and AN2) were discriminated based on their intensity of red (FL3) versus orange (FL2) autofluorescence. (B) Relative sizes of the 3 autotroph populations are illustrated in plots of side scatter verses chlorophyll autofluorescence

ial abundance was determined using a FACSCalibur. Samples for flow cytometry (FCM) were prefiltered through 50 µm mesh (Nitex), retained at 4°C in the dark and analysed within 4 h of collection. Regions were established in bivariate plots of scatter and/or fluorescent that best segregated particles with similar fluorescence (Fig. 1). The weight of the sample tube (±0.0001 g) was measured using a Mettler Toledo, 4 decimal place, balance before and after each analysis. The anolyte volume for each sample was then computed from the change in sample mass using a specific gravity for seawater of 1.025 and the volume analysed then used to convert event counts in each region into cell concentrations. PeakFlow Green 2.5 µm beads (Invitrogen) were also added to all samples as an internal standard to ensure that estimation of fluorescence emission did not change within and among samples.

The abundance of eukaryotes (phytoplankton and microheterotrophs) was determined at high flow rate (~60 µl min^{-1}) using 0.22 µm-filtered seawater as the sheath fluid. Pico- and nano-sized phytoplankton were detected by chlorophyll autofluorescence in fresh samples that were housed in a beaker of ice to avoid heat stress during analysis. Like Thomson et al. (2010), bivariate plots of red (FL3) versus orange (FL2) fluorescence were used to identify aggregations of phytoplankton cells with similar autofluorescent characteristics (Fig. 1). Heterotrophic nanoflagellates were determined using the methods of Rose et al. (2004) and Thomson et al. (2010) by staining 10 ml samples with 7.5 µl of a 75 nM working solution of LysoTracker green (Invitrogen) and incubating for 10 min in the dark. Heterotrophic nanoflagellates were discriminated from detritus, pico- and nanophytoplankton using a sequence of scatter plots as described by Rose et al. (2004) and Thomson et al. (2016).

The abundance of bacteria with high and low DNA content was determined from samples fixed to a final concentration of 0.5% glutaraldehyde for 1 h and stained for 20 min with 1:10000 dilution of SYBR-Green I (Invitrogen) (Marie et al. 1999). Samples were run for 3 min at a low flow rate (~35 µl min^{-1}) and bacterial abundance was determined from bivariate scatter plots of side scatter (SSC) verses green (FL1) fluorescence.

The relationship between particle size and the forward scatter value on the flow cytometers was determined using beads of known particle diameter. Forward scatter (FSC) values were obtained for 6 spherical beads ranging from 1.0 to 16.7 um diameter. Log/log regression of ESD vs. FSC gave a highly significant linear regression over this range in diameter ($r = 0.9906$, $df = 4$, $p < 0.01$).

Samples commonly contained 2 particles of known size, namely a 2.5 µm diameter green-fluorescent bead as an internal standard (see above) and a cryptophyte of measured size (average 9.76 µm ESD). These particles were readily identified by the high FL1 fluorescence of the beads and the high FL2 autofluorescence of phycoerythrin in the cryptophyte. Given the relationship between FSC and bead

diameter (above), a least-squares regression was performed for the log-transformed diameters of the 2 particles of known size (bead and cryptophyte). The regression formula and mean FSC value for each cytometric group (Fig. 1) was then used to calculate the average ESD for each region. We acknowledge that the refractive index of beads may have influenced our estimation of cells size.

Chl *a*

A known volume of seawater from each minicosm was filtered through 13 mm Whatman GF/F filters, the filter folded in half, blotted dry and immediately transferred to liquid nitrogen, transported to Australia and stored at −135°C in an ultralow freezer (Sanyo) until analysis within 7 mo. Pigments were extracted, analysed and quantified by HPLC following the protocol of Wright et al. (2010).

Particulate organic carbon (POC) and nitrogen (PON)

Concentrations of POC and PON were determined using samples prepared using the protocol of Pearce et al. (2007), except that samples were filtered onto a muffled 25 mm Sartorius Quartz microfibre filter (nominal pore size 0.8 µm) until the filter clogged. Sample analysis was performed using Carlo Erba Elemental Analyser at the University of Tasmania.

Statistical analyses

The minicosm experiment was based on a repeated-measures design in which the microbial abundances were measured in 6 unreplicated pCO_2 treatments. This design precluded formal statistical tests of the interaction between time and pCO_2 treatment. However, these interactions were evident from temporal trends in abundance of the individual microbes and from the grouping of samples over time and among treatments in cluster analyses, nonmetric multidimensional scaling (nMDS) and constrained canonical analysis of principal components (CAP) plots (see below). Subsampling of each minicosm provided within-treatment pseudoreplicates that were used to make an informal assessment of treatment effects. In all time-series plots, a small amount of random noise was added to the sample time to avoid over-plotting of data.

Raw microscope counts of microbial composition and abundance were grouped and transformed prior to statistical analysis. Cell abundances were then computed and $\log_{10}$ transformed to reduce the influence of abundant species and help normalise data distributions. Cluster analysis and ordination was then performed to visualise the similarity of samples in 2 dimensions. The Bray-Curtis index (Bray & Curtis 1957) was used to calculate the resemblance of samples based on the community structure. The resulting resemblance matrix was then used to perform an unconstrained ordination by nMDS, with a primary ('weak') treatment of ties (Kruskal 1964a,b). The nMDS was repeated over 50 random starts to ensure a globally optimal solution according to the Procrustes residual mean square error (Peres-Neto & Jackson 2001).

Cluster analysis (hierarchical agglomerative clustering) was performed based on the resemblance matrix (above) using the group-average linkage. Significant differences among sample clusters were determined according to the similarity profile permutation method (SIMPROF) of Clarke et al. (2008), based on alpha = 0.05 and 1000 permutations. SIMPROF identified 10 clusters of samples that differed significantly in microbial structure. Sample cluster groups were then superimposed on the nMDS ordination. In addition, the species scores (weighted averages of sample scores) were computed and added to the nMDS plot. As a result, the abundance the various microbes in a particular sample was represented by the proximity of each species to that sample in the nMDS plot: the closer the taxon to a sample, the more abundant it was in that sample (see Table 1 for abbreviations of microbial groups).

The CAP analysis was performed following the protocol of Oksanen et al. (2015) to assess the significance of known environmental covariates pCO_2, NO_x, SiO_4 and PO_4 (constraints) in determining the microbial community structure. This procedure again used the Bray-Curtis resemblance matrix but, unlike the nMDS, the method partitions total variance in community composition into unconstrained and constrained components, with the latter interpretable as the variation that can be attributed to the 4 covariates noted above. Random reassignment of sample resemblance over 199 permutations was used to compute the pseudo-*F* statistic as a measure of the significance of each environmental constraint in changing the structure of the microbial community (Legendre & Anderson 1999). In addition, a forward selection strategy was used to choose the minimum subset of constraints required to explain most of the

variation in the microbial community (Legendre et al. 2011). Goodness-of-fit for a final model was described using adjusted R^2 values after the recommendation of Peres-Neto et al. (2006).

Like the nMDS, species scores were added to the CAP plots to indicate the relative importance of each microbial taxa/group to each sample (see Table 1 for abbreviations). Blue arrows were been added to show the constraints that significantly correlated with changes in structure of the microbial community. The orientation of these arrows indicates the direction of increasing effect and their length reflects the relative magnitude of the effect on community structure. The assumption of a linear gradient in each constraint was checked by comparing the linear projections with 2-dimensional surfaces, and in all cases a linear approximation was found to be satisfactory.

All analyses were performed using R v3.2.1 (R Core Team 2015) and the add-on package vegan v2.3-1 (Oksanen et al. 2015).

RESULTS

Water chemistry

pCO_2

Adjustment and maintenance of pCO_2 gave 6 pCO_2 treatments. The lowest pCO_2 treatment was 84 ± 6.4 µatm, which approximated the ambient concentration of 107 µatm in the seawater when the tanks were filled. This ambient value was calculated from the measured TA of 2318 µM kg^{-1} seawater and TCO_2 of 1949 µM kg^{-1} seawater at an *in situ* temperature and salinity of 2.07°C and 33.708 PSU, respectively, and closely matched that calculated using TA or TCO_2 of the measured seawater pH 8.51 (109 µatm). Above this were 4 stepwise increases of ~600 µatm, reaching an average of 2432 ± 103.2 µatm. Standard errors increased with increasing pCO_2 concentration, reflecting the decreasing buffer capacity of seawater as the pCO_2 increased; however, the error as a proportion of the absolute concentration declined. Variation in CO_2 concentration in each treatment remained fairly constant during the experiment, with one exception. High rates of phytoplankton photosynthesis caused a noticeable drop (~40%) in pCO_2 between Days 5 and 6, despite the daily addition of CO_2-saturated seawater to compensate for this draw-down. This brief excursion was immediately corrected on Day 6.

Nutrients

Concentrations of NO_x fell from average values of 4.8 µM on Day 0 to 0.7 µM on Day 8 and were below the levels of detection by Day 10 (Fig. 2A). Similarly, concentrations of SRP fell from 4.50 µM on Day 0 to 0.65 µM on Day 8 and were undetectable by Day 10 (Fig. 2B). At higher pCO_2, concentrations of NO_x and SRP peaked following 6 d incubation but then declined to values only

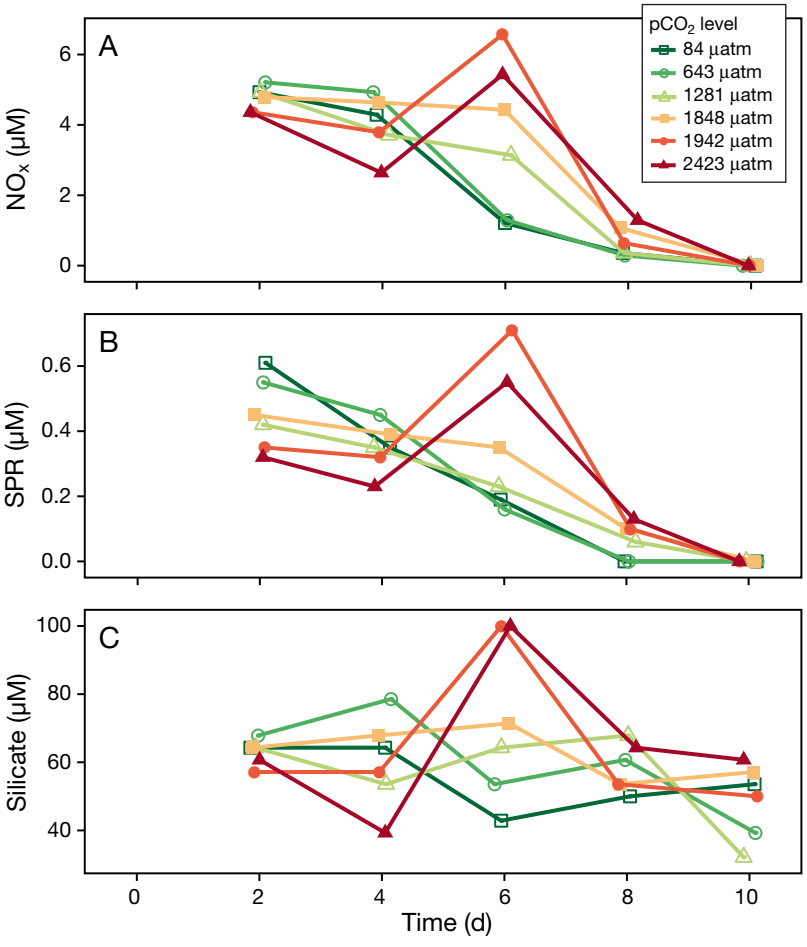

Fig. 2. Nutrient concentrations. Concentrations of dissolved (A) nitrate + nitrite (NO_x), (B) soluble reactive phosphorous (SRP) and (C) molybdate-reactive silicate (silicate) over 10 d incubation of a natural microbial community in tanks maintained at different pCO_2 levels. Note different *y*-axes

slightly higher than those in treatments exposed to ≤1281 µatm CO_2. In contrast, silicate concentration declined from an average of 63.1 to 48.8 µM on Day 10 but varied more among treatments at each time. The rate of decline was highest between Days 4 and 6 in low-pCO_2 treatments (≤643 µatm), but concentrations increased at this time in higher pCO_2 treatments (Fig. 2C). Detection limits of the analysis method for NO_x and silicate comprised only 3.0 and 5.7%, respectively, of the average concentrations on Day 2. Thus, the limits of detection had little effect on interpretation of the data for these nutrients. This contrasted with the detection limits for SRP, which comprised 21.4% of average measured concentrations. Average values of nutrient draw-down for N:P:Si were 10.6:1:12.4 on Day 8, prior to NO_x and SRP falling to undetectable levels.

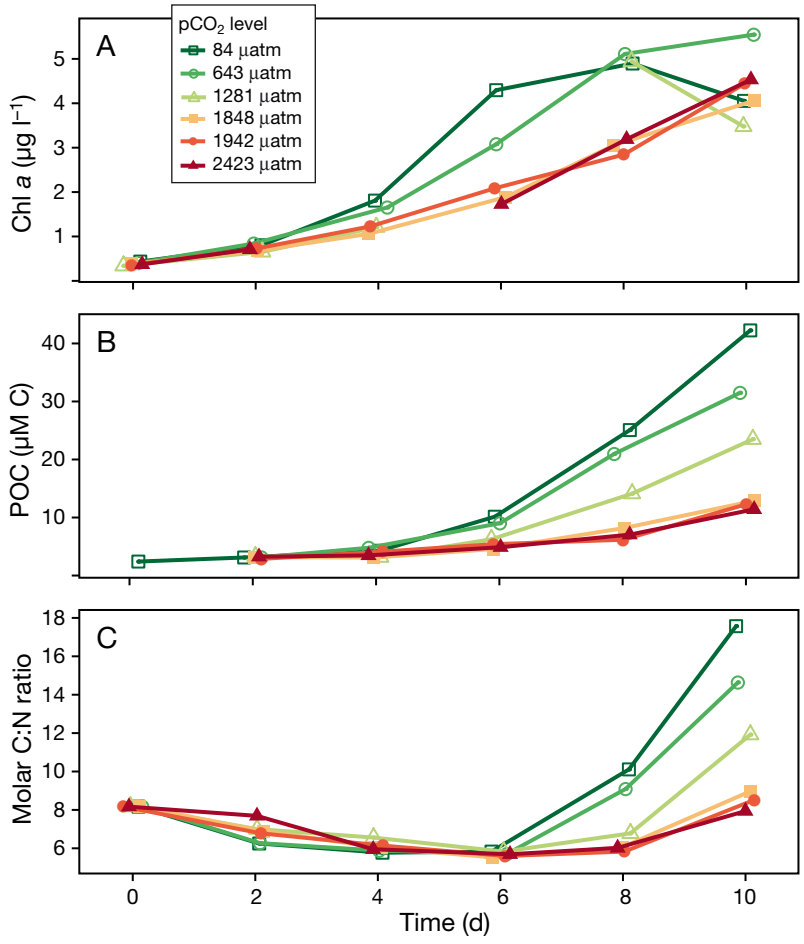

Fig. 3. Microbial biomass and elemental composition. Concentrations of (A) chlorophyll *a*, (B) measured particulate organic carbon (POC) and (C) molar ratio of particulate organic carbon to nitrogen (C:N ratio) over 10 d incubations of a natural microbial community in tanks maintained at different pCO_2 levels. Note different *y*-axes

Bulk biological parameters

Changes in the concentrations of chl *a* and POC showed a strong dose response to CO_2. Concentrations of chl *a* increased exponentially from the beginning of the experiment in all CO_2 treatments (Fig. 3A). Low-pCO_2 treatments (≤643 µatm) had the highest rate of chl *a* increase, which peaked at about 5 µg chl *a* l^{-1} on Day 8 at the onset of nutrient exhaustion (Fig. 2), and slowed or declined thereafter. Concentrations in high-pCO_2 treatments (≥1848 µatm) grew more slowly and reached final concentrations similar to the low-pCO_2 treatments, but without slowing or declining during the experiment.

Concentrations of POC increased exponentially throughout the experiment in all treatments and differed greatly among treatments on Days 8 and 10 (Fig. 3B). On Day 8, concentrations of POC in high-pCO_2 treatments (≥1848 µatm) differed little, ranging from 6.2 to 8.2 µM C l^{-1}, and increased slightly to 11.4–12.9 µM C l^{-1} on Day 10. In contrast, in lower pCO_2 treatments (≤1281 µatm) the rate of POC accumulation increased as the CO_2 concentration declined among treatments, reaching 25.1 µM C l^{-1} and 42 µMC l^{-1} in the 84 µatm treatment on Days 8 and 10, respectively.

Molar ratios of POC to PON (C:N) declined around 25% from approximately 8.2 to 5.7 in all treatments during the first 6 d of incubation, (Fig. 3C). In low-pCO_2 treatments (≤643 µatm) the C:N ratio then increased after Day 6, rising to between 9.1 and 10.1 on Day 8 and reaching 14.7 to 17.6 on Day 10. In high-pCO_2 treatments (≥1848 µatm) C:N ratios were ~6 following 8 d incubation and increased slightly on Day 10, reaching 7.9 to 9.0. The C:N ratios in the treatment exposed to 1281 µatm fell between the extremes in the high- and low-pCO_2 treatments.

Microbial community structure

Microscopy (Fig. 4) and flow cytometry (Fig. 5) showed that most microbial taxa/groups had a consistent dose-related response to enhanced CO_2 and that this was strongly related to cell size (Table 1).

The abundance of most large diatoms, namely those averaging >11 µm in ESD,

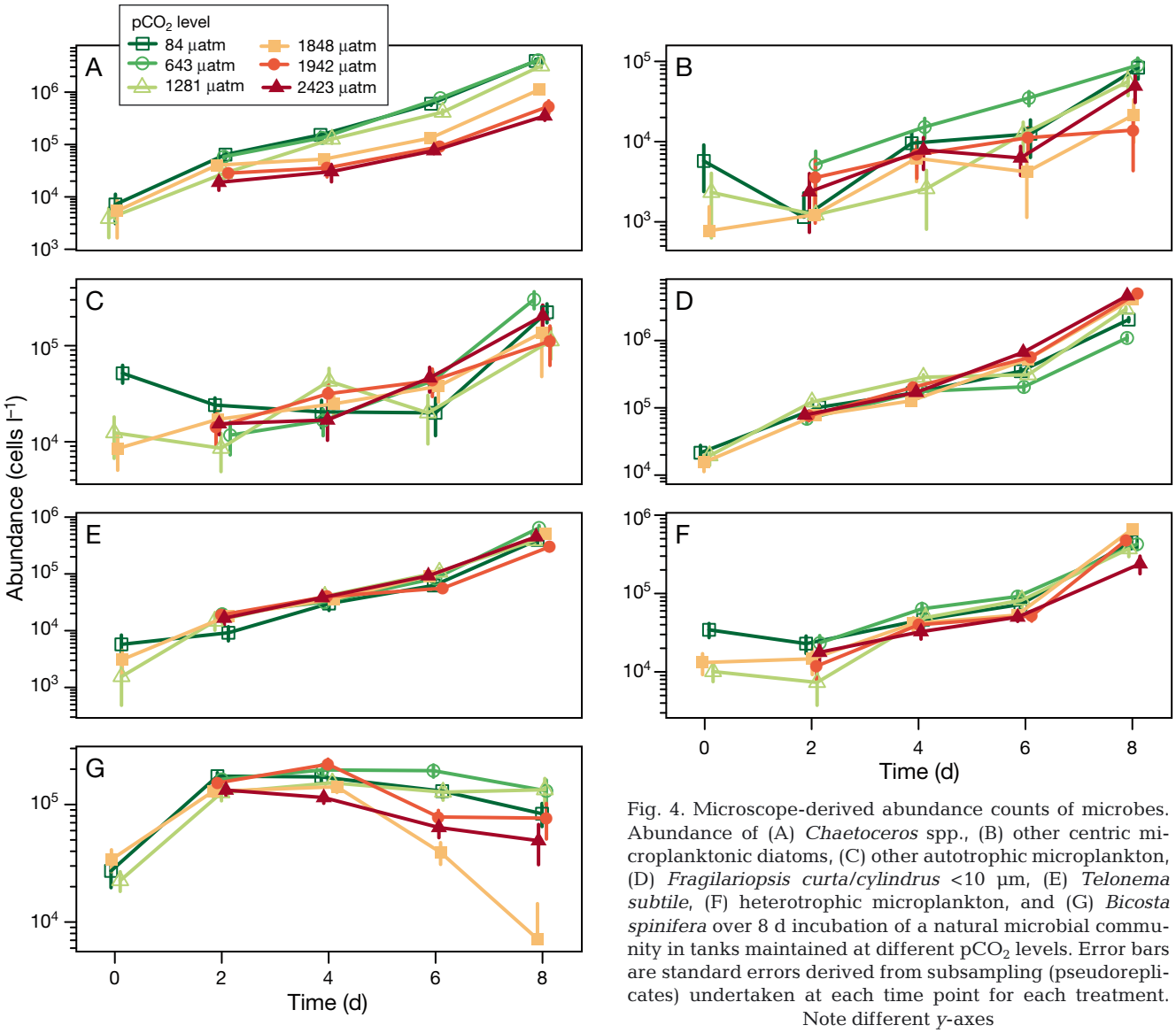

Fig. 4. Microscope-derived abundance counts of microbes. Abundance of (A) *Chaetoceros* spp., (B) other centric microplanktonic diatoms, (C) other autotrophic microplankton, (D) *Fragilariopsis curta/cylindrus* <10 µm, (E) *Telonema subtile*, (F) heterotrophic microplankton, and (G) *Bicosta spinifera* over 8 d incubation of a natural microbial community in tanks maintained at different pCO_2 levels. Error bars are standard errors derived from subsampling (pseudoreplicates) undertaken at each time point for each treatment. Note different *y*-axes

increased quickly under low pCO_2 and very slowly under high pCO_2. These included *Chaetoceros* spp., other centric microplanktonic diatoms (mainly *Eucampia antarctica* var. *recta*, *Proboscia* spp. and a range of unidentified taxa), and other autotrophic microplankton (mainly *Navicula glacei* var. *parvula*, *Pseudonitzschia subcurvata*, and autotrophic dinoflagellates, Figs. 4A–C, respectively).

Most small taxa (<5 µm ESD) had the opposite response to that of the large diatoms. Their abundance increased quickly under high pCO_2 and more slowly or declined under low pCO_2, but with a variety of patterns. The abundance of *Fragilariopsis curta/cylindrus* (<10 µm long and averaging 4.6 µm ESD) increased exponentially in all treatments but faster in high-pCO_2 treatments (Fig. 4D), while that of autotrophic nanoplankton 1 increased in all treatments before growth stopped in the low-pCO_2 treatments (Fig. 5A). In contrast, the abundance of the smallest cells declined under low pCO_2, namely autotrophic picoplankton, high- and low-DNA content bacteria (Figs. 5C–E, respectively), but fell after the early peak in autotrophic picoplankton and high-DNA content bacteria at high pCO_2 (Figs. 5C,D). Heterotrophic nanoflagellates had a different response (Fig. 5F). They grew fastest in low pCO_2, and the abundance in all treatments peaked and then fell, though later and with smaller peak in abundance under high-pCO_2 treatments. The nanoplanktonic heterotroph *Bicosta spinifera* had a similar response, although the difference in treatments occurred later in the experiment (Fig. 4G).

Some taxa had no apparent growth response to pCO_2: *Telonema subtile*, heterotrophic microplank-

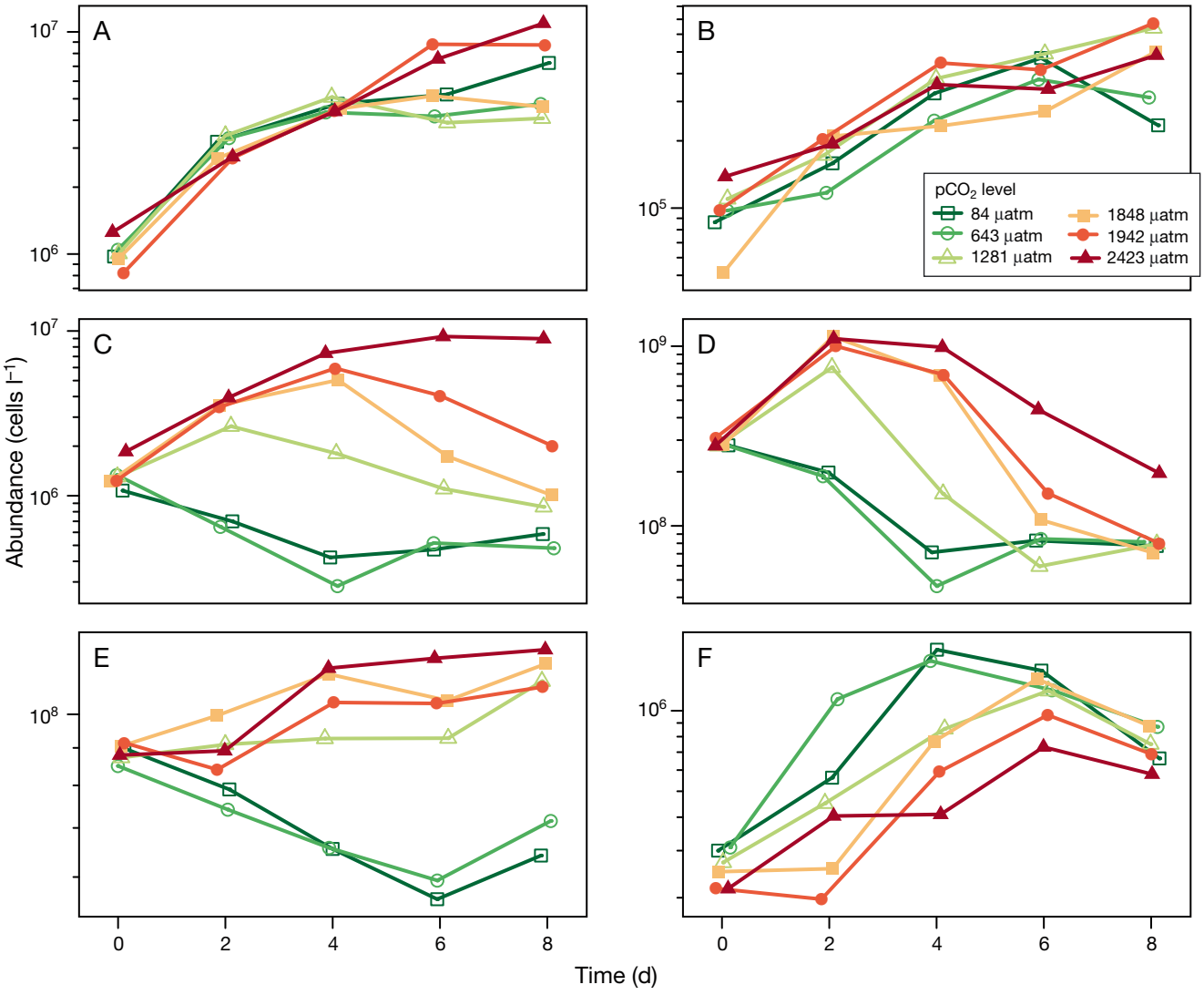

Fig. 5. Flow cytometry-derived abundance of microbes. Abundance of (A) autotrophic nanoplankton 1, (B) autotrophic nanoplankton 2, (C) autotrophic picoplankton, (D) high-DNA content bacteria (E) low-DNA content bacteria, and (F) heterotrophic nanoflagellates over 8 d incubation of a natural microbial community in tanks maintained at different pCO_2 levels. Note different *y*-axes

ton spp. (mainly *Gyrodinium* spp.) and autotrophic nanoplankton 2 (Figs. 4E, 4F, 5B, respectively).

Cluster analysis showed that most of the change in the microbial community occurred among sampling times. SIMPROF also showed that within each time point, the microbial community was consistently divided into 2 significantly different structural states; those exposed to high (≥1848 µatm) and low (≤643 µatm) pCO_2 (Fig. 6A). The treatment exposed to 1281 µatm was grouped with the low-pCO_2 treatments on Days 0, 6 and 8 but with high-pCO_2 treatments on Days 2 and 4, suggesting that its microbial community was intermediate between the 2 structural states.

nMDS and cluster analysis gave equivalent groupings of samples based on microbial composition (Fig. 6B). The stress value of 0.05 obtained for the nMDS showed that it adequately resolved the dissimilarity among samples in 2 dimensions. Samples were ordered sequentially through time on axis 1 and CO_2 treatment on axis 2. Importantly, heterotrophic nanoflagellte and *Bicosta spinifera* abundance was high in samples that were briefly exposed (2 to 4 d) to low pCO_2. Longer exposures to low pCO_2, led to a community composed largely of microplankton, including other autotrophic microplankton, heterotrophic microplankton, other centric microplanktonic diatoms and *Chaetoceros* spp. In con-

Table 1. Microbial group abbreviations and sizes. Abbreviations and equivalent spherical diameters (ESD) of taxa and functional groups of marine microbes. Protist taxa/groups were categorised as microplanktonic (marked *) if their longest cell dimension exceeded 20 µm. Thus, some microplanktonic groups (e.g. pennate diatoms) grouped in other autotrophic microplankton had an ESD much smaller than 20 µm

Data source	Taxon/group	Abbreviation	Average ESD (µm)
Microscopy	*Chaetoceros* spp.	Ch	12.3
	Other centric microplanktonic diatoms*	CM	53.8
	Fragilariopsis curta/cylindrus	Fc	4.6
	Telonema subtile	Ts	10.9
	Bicosta spinifera	Bs	4.8
	Other autotrophic microplankton*	AM	22.7
	Heterotrophic microplankton*	HM	31.1
Flow cytometry	Autotrophic picoplankton	AP	2.8
	Autotrophic nanoplankton 1	AN1	5.0
	Autotrophic nanoplankton 2	AN2	7.7
	Heterotrophic nanoflagellates	HNF	4.1
	High-DNA content bacteria	HB	0.9
	Low-DNA content bacteria	LB	0.8

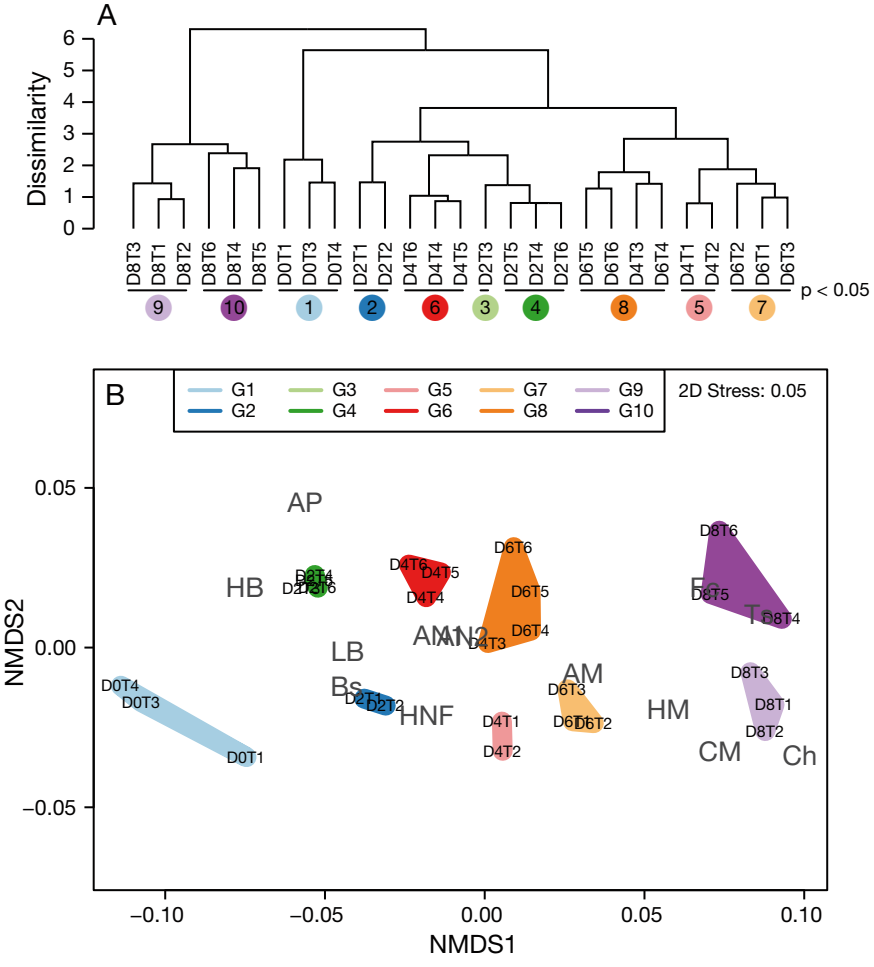

trast, exposure to high pCO_2 led to a community that was dominated by nano- and picoplankton, namely high DNA content bacterial, then — as the exposure increased — autotrophic picoplankton, low-DNA content bacteria and *Fragilariopsis curta/cylindrus* <10 µm. Intermediate to these were taxa of low sensitivity to enhanced CO_2 concentration, namely autotrophic nanoplankton 1 and 2 and *Telonema subtile*.

CAP analysis showed that the trajectory of community succession over time clearly differed among pCO_2 treatments (Fig. 7). CAP axes 1 and 2 were highly significant in depicting the variance among samples due to the environmental constraints (pCO_2, NO_x, SRP and silicate) (Table 2). The magnitude of the change in trajectory was determined by the CO_2 concentration, and the differences in microbial community structure among CO_2 treatments were significant (Table 3). Arrows representing the linear projections of the 3 significant constraints in the CAP plot show that NO_x and silicate closely aligned with CAP axis 1. Changes in these constraints along this axis reflect nutrient depletion over time and coincide with increasing duration of sample incuba-

Fig. 6. Multivariate cluster analysis and nMDS based on similarity in microbial biomass among CO_2 treatments and times. (A) Cluster analysis based on the microbial community structure showing 10 significantly different groups obtained by SIMPROF (denoted by black lines beneath sample labels). Samples are abbreviated according to days of incubation (D0–8) and level of pCO_2 treatment (T1–6 for 84, 643, 1281, 1848, 1942, and 2423 µatm, respectively). (B) nMDS plot structure showing in 2 dimensions the unconstrained ordination of dissimilarities in microbial community structure with time (D0–8) and increasing CO_2 treatments (T1–6), overlayed with weighted-averages of the day–treatment scores for each microbial taxa/functional group (see Table 1 for abbreviations of microbes). Colours reflect the 10 cluster groups (G1–10) identified by SIMPROF

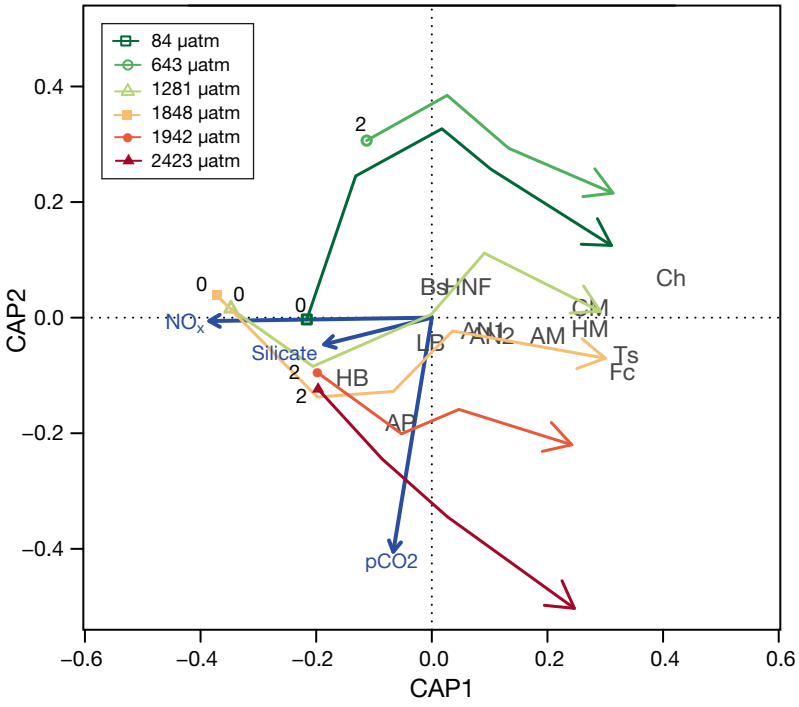

Fig. 7. Canonical analysis of principal coordinates (CAP) based on the similarity in microbial community structure among CO_2 treatments and times, showing the trajectory of change in the microbial community for each pCO_2 level (coloured arrows) based on the biomass of the component taxa/functional groups. Arrow starting points are labelled with the first sampling day for each treatment and all arrows end on Day 8 of the experiment. Microbial group scores were added to the CAP as weighted averages of sample scores (see Table 1 for abbreviations), and linear projections of significant constraints NO_x, silicate and pCO_2 appear as blue linear arrows

tion. The arrow for pCO_2 is approximately orthogonal and closely aligned with axis 2. In contrast to the unconstrained ordination (nMDS, Fig. 6B), CAP showed a clear separation of CO_2 treatments on axis 2. Overall the CAP analysis, based on the constraints pCO_2, NO_x, SRP and silicate, provided a model with 2 significant axes that together accounted for 74.3% of the variation in similarity among samples ($F_{4,22}$ = 16.086, p < 0.005 based on 199 permutations) (Table 2). However, marginal effects showed SRP was not significant ($F_{1,22}$ = 1.0494, p > 0.40 based on 99 permutations), and dropping this term provided a simplified model that still accounted for 73.3% of the total inertia. All remaining terms were highly significant (p < 0.005) and accounted for 12% (pCO_2), 71% (NO_x) and 17% (silicate) of the variance explained by the 3 constraints (Table 3, Fig. 7).

Table 2. Canonical analysis of principal coordinates (CAP) axis significance against covariates. Permutation tests assessing the significance of each constrained axis in CAP using the covariates pCO_2, NO_x, silicate and soluble reactive phosphorous as constraints upon community structure. Significance tests of the CAP axes are conditional on previous constrained axes in the model

	df	Variance	*F*	No. perm	Pr (>*F*)
CAP1	1	0.0227008	54.7835	199	0.005
CAP2	1	0.0026795	6.4663	199	0.005
CAP3	1	0.0012029	2.9030	199	0.015
Residual	23	0.0091162			

Table 3. Permutation tests assessing the significance of each environmental covariate (constraint) in determining microbial community structure using principal coordinates (CAP), showing significant marginal effects for pCO_2, NO_x and silicate

	df	Variance	*F*	No. perm	Pr (>*F*)
pCO_2	1	0.0030148	7.2599	199	0.02
NO_x	1	0.0187336	45.1127	199	0.01
Silicate	1	0.0044798	10.7880	199	0.01
Residual	23	0.0095510			

DISCUSSION

Our study showed that natural communities of Antarctic marine microbes were resilient to changes in pCO_2 from 84 to 643 µatm, but higher pCO_2 levels, predicted near the end of this century (IPCC 2014), reduced the overall rates of biomass accumulation (chl *a* and POC) and changed the community structure, favouring smaller phytoplankton. To understand the effect of increasing pCO_2 levels on this Antarctic microbial community, we first consider the experimental approach, then the effects of pCO_2 on microbial community structure and abundance, and finally the CO_2-induced effects on community-level interactions and the potential consequences for ecosystem services in Antarctic coastal waters.

Experimental approach

Our experiments covered a broad range of CO_2 concentrations encompassing those from pre-industrial times to that predicted post-2300. The lowest treatment in our experiment approximated the ambient seawater CO_2 concentration of 107 µatm at the time the experiment began. This low *in situ* pCO_2 concentration in the near-shore seawater at Davis Station was likely due to the draw-down of CO_2 by the spring phytoplankton bloom in water advected to our sample site and the melting of sea ice that is undersaturated in CO_2 (Gibson & Trull 1999). The highest treatment approximated the maximum ocean CO_2 concentration predicted for approximately 2300 by Caldeira & Wickett (2003) using the IPCC-AR4, IS92a business as usual scenario.

The addition of CO_2-saturated seawater to adjust the CO_2 concentrations in the minicosm tanks is an accepted means of simulating the effects of ocean acidification on the carbonate chemistry and has been used in the recent EPOCA experiments in Kongsfjorden (e.g. Schulz et al. 2013). This technique also avoided damage of small delicate protists (such as naked flagellates) by bubbling (Iglesias-Rodriguez et al. 2008, Shi et al. 2009), which may have contributed to previous reports of large, robust diatoms being favoured at high pCO_2.

We maintained the pCO_2 during our experiment, unlike previous mesocosm studies that adjusted the CO_2 to target concentrations at the start of their experiment, after which it was allowed to change due to photosynthesis and respiration (e.g. Riebesell et al. 2007, Schulz et al. 2013). Our approach allowed us to quantify the effect of sustained CO_2 concentrations on the marine microbial community and estimate the critical thresholds of pCO_2 that elicit changes in community structure and function.

The lamps used to illuminate the minicosms were comparable in wavelength and intensity to ambient solar radiation at Davis Station (see 'Materials and methods: Minicosm operation'). However, the experimental light climate did not simulate natural variations in solar irradiance due to changes in time of day, season, weather, albedo, or absorbance by particulate or dissolved matter in the water column. The absence of this variability may have elevated rates of phytoplankton productivity in high-pCO_2 treatments as it avoided the CO_2-induced decrease in light-use efficiency of cells exposed to a variable, but not constant, light climate (Hoppe et al. 2015).

While we measured all parameters for the entire 10 d of the experiment, we restricted our analysis of the microbial community to the period that macronutrient concentrations supported phytoplankton growth in all treatments. In low-pCO_2 treatments (≤1281 µatm) chl *a*, carbon and abundant protists plateaued or declined following >8 d incubation, nitrogen concentrations were below detection, and C:N ratios increased, showing that macronutrient availability limited their growth. Thus, changes in community structure at ≥1848 µatm were only affected by pCO_2, while communities at ≤1281 µatm were simultaneously affected by both pCO_2 and macronutrient availability. Thus, to avoid confounding our ability to detect CO_2 response by simultaneously exposing some treatments, including the control (ambient pCO_2), to nutrient effects on Day 10, we only compared the microbial structure among treatments over the first 8 d of minicosm incubation.

Compared to the PeECE and KOSMOS experiments in Norwegian coastal waters, which used mesocosms of up to ~53 000 l (e.g. Schulz et al. 2008, 2013), our 650 l minicosms potentially suffered more severely from the accepted limitations of mescosm-style studies. Such limitations include that they experience greater wall effects, and deviations of the incubated community from nature may expose cells to unnatural levels of physical turbulence and excluded any organisms >200 µm in length (Kim et al. 2008). Such factors probably contributed to the initial decline in species richness in all minicosm tanks, irrespective of pCO_2 treatment (data not shown) and the rapid accumulation of biomass in our tanks (see below).

Our experiments did not acclimate microbes to the target CO_2 concentrations and may have overestimated the sensitivity of the community to ocean acidification and/or precluded the expression of positive effects of enhanced pCO_2. We adjusted the CO_2 to the target concentration in a single step over ~2 h. Exposing cells to such a rapid and potentially stressful environmental change can cause a large and sudden drop in fitness by restricting the expression of phenotypic plasticity and selection of genotypes that better tolerate high pCO_2 (Collins & de Meaux 2009, Chevin et al. 2013, Schaum et al. 2013). Yet waters near our study site reportedly experience large and rapid natural changes in carbonate chemistry (Gibson & Trull 1999, McNeil et al. 2011, Roden et al. 2013). Occupancy of such a variable environment can reportedly select organisms (species and strains) with high physiological plasticity (Chevin et al. 2013, Schaum et al. 2013). This agrees with our study which, despite the absence of acclimation, showed no significant difference in the microbial community

among treatments exposed to pCO_2 levels from 84 to 643 µatm (see below). Alternatively, the absence of an acclimation period may have precluded expression of beneficial effects of enhanced pCO_2 on Antarctic marine microbes including the increased cell size, growth, and productivity reported by Tortell et al. (2008), Feng et al. (2010), Torstensson et al. (2013) and Trimborn et al. (2013).

Finally, our removal of metazooplankton undoubtedly increased the rate of biomass accumulation in our study but also removed effects of pCO_2-induced changes in grazing by higher trophic levels. Zooplankton reportedly differ in their sensitivity and response to elevated pCO_2, likely causing changes in the rate, size and characteristics of microbes they consume as CO_2 concentration increases (Saba et al. 2012, Kawaguchi et al. 2013, Cripps et al. 2014). Thus, while trophic-level interactions among members of the microbial loop are included in our study, those between microbes and higher trophic levels are not.

Response to CO_2

Our study showed that CO_2 concentrations can significantly alter the structure of Antarctic microbial communities (phytoplankton, protozoa and bacteria) and that the threshold for this response was between 643 and 1281 µatm. Univariate graphs of bulk parameters (Fig. 3) and many protist taxa and groups (Figs. 4 & 5) showed clear dose-responses. These trends were further illustrated by exploratory analyses (sample groupings in cluster and nMDS analyses and CAP trajectories) (Figs. 6 & 7). While both exploratory and univariate analyses showed that the primary factor responsible for the structure of the microbial community was time (sample day or nutrient concentration as its proxy), consistent CO_2-induced changes were also observed. Communities exposed to CO_2 concentrations of 84 µatm (ambient) and 643 µatm remained strongly similar as they grew. These treatments approximated 0.2 to 1.7 times average atmospheric pCO_2 when the experiments were performed. CO_2 concentration ≥1281 µatm exceeded the tolerance threshold of the microbial community, resulting in changes to the community structure, favouring small protists (<5 µm ESD) over large taxa, and reducing the rate of chl *a* and POC accumulation (Figs. 3 to 7). The significance of these changes in microbial structure were confirmed by non-parametric permutational statistics (SIMPROF and CAP pseudo-*F*) (Fig.6, Table 3).

Phytoplankton

The large range we observed in CO_2 tolerance of Antarctic phytoplankton (84 and 643 µatm) is perhaps unsurprising, given the seasonal extremes in ambient CO_2 in Antarctic coastal waters (e.g. Gibson & Trull 1999, McNeil et al. 2011, Roden et al. 2013). RuBisCO, the carbon fixation enzyme in photosynthesis, has a low affinity for CO_2 and a half-saturation constant well above that in seawater and anthropogenic enhancement of ocean pCO_2 can potentially enhance rates of phytoplankton photosynthesis (e.g. Rost et al. 2008). Yet many of the phytoplankton taxa studied have highly regulated carbon concentrating mechanisms (CCMs), which mitigate limitation of photosynthesis by CO_2 supply (Giordano et al. 2005, Roberts et al. 2007). Like previous studies, we found no evidence that the phytoplankton in our study were limited by CO_2 availability, despite exposure to concentrations as low as 84 µatm (Burkhardt et al. 2001, Rost et al. 2003, 2008). Thus, it is plausible to hypothesise that the phytoplankton in our study had acquired attributes that better suit them to their environment (adaptations) such as CCMs, which conveyed a low sensitivity to the large changes in pCO_2 they encounter in their natural environment (e.g. Hinga 2002, Joint et al. 2011).

Instead of elevated pCO_2 enhancing growth, we found that it slowed accumulation rates of chl *a* and carbon. The reason(s) for this inhibition are unclear. It may be due to direct effects of elevated CO_2 and pH on cells and/or the energetic costs of mitigating these changes in intracellular chemistry via such tolerance strategies and proton pumps (e.g. Lohbeck et al. 2014). Alternatively, recent studies show that the CO_2-induced production of signal molecules that down-regulate production of CCMs can also suppress photosynthesis, respiration and general cell metabolism (Hennon et al. 2015).

The lower total biomass and increased relative abundance of small microbes we observed in high-pCO_2 treatments differed from most previous studies, including the few that have been conducted in Antarctic waters (Tortell et al. 2008, Feng et al. 2010). Instead, they were similar to those from the Bering Sea (Hare et al. 2007) and communities from nutrient-limited Norwegian waters (Brussaard et al. 2013, Schulz et al. 2013) where small protists dominated at high CO_2 concentrations. Yet nutrients were not initially limiting in our study, suggesting the CO_2-induced changes we observed were due to other factors such as changes in top-down control by nano- and microzooplankton grazing or iron limitation (see below, Thomson et al. 2016) .

Uptake ratios of NO_x, SRP and silicate by phytoplankton in our study were similar to those reported for diatom blooms (Harrison et al. 1977, Brzezinski 1985). The high variability in nutrient concentrations among treatments may be due to changes in the abundance of heterotrophic nanoflagellates and bacteria (Fig. 4) and their effect on nutrient recycling and/or differences in the nutrient demand and uptake kinetics of diatoms of different taxa and size (Guillard & Kilham 1977, Pomeroy et al. 2007, Pearce et al. 2008). However, it is also possible that the elevated nutrient concentrations on Day 6 may be due to contamination, either of the nutrient samples themselves or of the CO_2-bubbled seawater that was added to the minicosms to maintain the experimental CO_2 concentration.

Unlike in previous studies, we found ratios of C:N were highest in low-pCO_2 treatments. Carbon overconsumption can reportedly increase ratios of C:N at high pCO_2 (e.g. Burkhardt et al. 1999), as can an increase in the relative abundance of small taxa (Putland & Iverson 2007). Instead we found C:N reflected the faster phytoplankton growth and depletion of nutrients in low-pCO_2 treatments. Thus, this ratio was determined by limited availability of nitrogen rather than the higher availability of carbon. This was reinforced by the continued exponential increase in POC in low-pCO_2 treatments between Days 8 and 10, despite a coincident plateau or decline in chl *a* concentrations (Fig. 2).

A CO_2-induced decline in iron availability may also contribute to the dominance of small cells in high-pCO_2 treatments. We calculate that only 0.3 nM of the 5 nM iron added would have been used, based on the observed reduction of dissolved N and assuming C:Fe = 1.5×10^5 (Gregg et al. 2003) and C:N = 6.6 (Redfield 1934). However, the effect of elevated CO_2 concentration on biological iron availability remains contentious, with Shi et al. (2010) reporting iron declined, while Millero et al. (2009) calculated it would increase. Much of the iron in the ocean is bound to siderophores and other ligands, upon which the effects of enhanced CO_2 remain unclear (Hoffmann et al. 2012). We added iron as FeEDTA and its chelation may have limited bioavailability. Thus, it remains possible that, despite having added iron to our minicosms, the low rates of biomass accumulation, lower rates of macronutrient depletion and higher relative abundance of small phytoplankton cells in the high-pCO_2 treatments were at least partly caused by iron limitation. If so, our results differ from Hoppe et al. (2013), who showed that elevated pCO_2 did not affect natural communities of Antarctic phytoplankton under iron-limited conditions.

Protozoa

Univariate graphs, nMDS and CAP analysis (Figs. 3F, 6 & 7) showed that CO_2 concentration had little effect on the abundance of heterotrophic microplankton but elevated concentrations coincided with limited growth of heterotrophic nanoflagelltes between Days 2 and 6. The insensitivity of heterotrophic microplankton to CO_2 concentration agrees with the few prior studies of these microheterotrophs (e.g. Suffrian et al. 2008, Aberle et al. 2013). In contrast, growth of heterotrophic nanoflagellates was slower in high-pCO_2 treatments (≥1281 µatm) on Days 2 to 6 (Fig. 5F). This slowed growth coincided with higher abundances of picoplankton (autotrophic picoplankton and bacteria), which are their potential prey (see below, Thomson et al. 2016). Thus, like studies of UV-B-induced changes in phytoplankton grazing mortality by Bothwell et al. (1994), our results indicate that increases in pCO_2 may alter trophic level interactions in the microbial loop with ramifications for the structure, size, abundance and biomass of phytoplankton.

To our knowledge, this limitation of heterotrophic nanoflagellte growth at elevated CO_2 is amongst the first observations showing an effect of CO_2 concentration on protozoa. Unlike Gong et al. (2010), we saw no evidence in our SEM preparations that pH effected lorica formation by choanoflagellates. Instead, the slower growth may be due to CO_2 narcotising cells into low metabolic rates or interruption of flagella function (Havenhand & Schlegel 2009, Morita et al. 2010). The similarity in heterotrophic nanoflagellte abundance among CO_2 treatments on Day 8 may be due to the higher abundance of picoplanktonic prey (autotrophic picoplankton and bacteria) compensating for CO_2-induced limitation of their growth or acclimation of the heterotrophic nanoflagelltes to elevated pCO_2.

Little is known about the direct effects of elevated CO_2 concentrations on protozoan abundance, growth or grazing rates (Caron & Hutchins 2013). Protozoans critically influence the structure, productivity and carbon flow in microbial communities (Pearce et al. 2008 and refs therein). The abundance and role of heterotrophic nanoflagelltes in the microbial food web is often hard to quantify. By definition heterotrophic nanoflagelltes are small, delicate and readily disrupted by manipulation and preservation. In addition, their identity is often cryptic and their trophic status is often hard to determine by light microscopy (e.g. Kuipers & Witte 1999). The mechanism/s by which enhanced CO_2 limits growth of heterotrophic

nanoflagelltes remain unknown but may include the indirect effects of CO_2 on heterotrophic nanoflagellte mortality via viral infection and/or grazing by microzooplankton (Larsen et al. 2008).

Bacteria

The abundance of high- and low-DNA content bacteria increased in treatments exposed to high pCO_2 levels and declined at low pCO_2 levels (Fig. 4E,F). Their location in the CAP analysis was strongly associated with the high-pCO_2 treatments (Fig. 7). This enhancement of their abundance was gradual but continuous for low DNA content bacteria but rapid and short lived (2 to 6 d) for high-DNA content bacteria. Our finding agrees with Maas et al. (2013), who found bacteria from the Ross Sea can adapt rapidly to increased pCO_2 by increasing their abundance and enzyme activity. High-DNA bacteria comprised most of the bacterial community in our study and are reportedly composed of larger taxa and/or cells that are metabolically active (Vila-Costa et al. 2012). It is unsurprising that active cells might respond more to the CO_2 treatment than those that were inactive, but this finding differed from Maas et al. (2013), who found the abundance of active cells declined with increasing pCO_2. Such differences among studies are likely due to differences in the methods used to estimate the abundance of active cells, availability of substrate or composition of the community (below). The effects of CO_2 concentration on the taxonomic composition of the bacterial community remain unclear (Roy et al. 2013, Sperling et al. 2013, Zhang et al. 2013). Of the few studies of CO_2 concentration on natural bacterial communities, Roy et al. (2013) found it had little effect on community composition. In contrast, Maas et al. (2013) found the diversity of the bacterial community declined with increasing pCO_2 while others have shown enhanced pCO_2 has variable or inhibitory effects on bacterial metabolism and exoenzyme activity (Yamada & Suzumura 2010, Motegi et al. 2013). Increasingly, studies show that the heterotrophic bacterial community is more active, productive and diverse at high CO_2 concentrations, responses which were attributed to an increase in phytoplankton biomass and production at high-pCO_2 in these studies and the consequent increase in substrates for bacterial growth (Piontek et al. 2010, 2013, Sperling et al. 2013). Instead, our results show that the accumulation of chlorophyll and POC was lower in the high-pCO_2 treatments (Fig. 3A).

Ecosystem-level effects

If indicative of future responses by natural communities, the decline in the size and biomass of phytoplankton we observed at elevated pCO_2 could threaten availability of carbon to higher trophic levels in the Antarctic food web. Large phytoplankton contribute much of the production and biomass in Antarctic blooms and fuel the 'food chain of giants' that substantially supports the wealth of life for which Antarctica is renowned (Smetacek 2008). The Antarctic krill *Euphausia superba* can only graze efficiently on particles ≥10 µm long and are reportedly unable to capture cells <6 µm in length (Boyd et al. 1984, Kawaguchi et al. 1999). Our study showed many of the microbes that dominated at high pCO_2 were commonly ≤5 µm ESD (Table 1). Krill are a keystone species in the Antarctic food web and any decline in their grazing efficiency would reduce their abundance, with ramification for higher trophic levels.

Our results tentatively suggest that concentrations CO_2 predicted beyond the end of this century (IPCC 2014) may also jeopardise other critical ecosystem services including the draw-down of atmospheric carbon and the efficiency of the biological pump. The lower rate of biomass accumulation we observed at high pCO_2 would reduce its depletion in near surface waters by photosynthesis and decrease the rate of dissolution of atmospheric CO_2 into the ocean (solubility pump) (e.g. Brévière et al. 2006, Gehlen et al. 2011). An increase in the relative abundance of small phytoplankton taxa is likely to lead to a decline in the abundance of large, rapidly settling, particles, and a subsequent decline in the efficiency of the biological pump would reduce sequestration of carbon to the deep ocean (Passow & Carlson 2012, Caron & Hutchins 2013). Small, slower sinking particles would be more likely to be respired in near-surface waters, raising CO_2 levels and either releasing CO_2 to the atmosphere or further reducing the solubility gradient from the atmosphere to the ocean. Thus, our study suggests that CO_2-induced changes in the microbial loop could alter the biogeochemistry in Antarctic waters and have a positive feedback on global warming.

CONCLUSIONS

Returning to the original questions posed in this study:

(1) Our experiment showed that enhanced concentrations of CO_2 significantly changed the abundance,

biomass and structure of the Antarctic marine microbial community we incubated. The threshold for this response was between 643 and 1281 µatm pCO_2. Below this threshold, phytoplankton communities were dominated by large diatoms and rates of biomass accumulation were relatively high. Above this threshold, communities were dominated by small taxa and rates of biomass accumulation slowed.

(2) Changes in the structure of the community were rapid, being initiated in the first few days of the experiment.

(3) Our results suggest that changes in the microbial community are likely to be due to a combination of direct effects of pCO_2/pH on the growth of component species and/or pCO_2-induced effects on interactions among trophic levels in the microbial loop. They also suggest that CO_2 concentrations predicted by around the end of this century (IPCC 2014) may elicit changes in Antarctic microbial communities that could jeopardise critical ecosystem services.

Acknowledgements. This work was supported by the Australian Antarctic Science projects AAS 40 and 4026 at the Australian Antarctic Division (AAD) and the Australian Government's Cooperative Research Centre's Program through the Antarctic Climate and Ecosystems Cooperative Research Centre (ACE CRC). We gratefully acknowledge the assistance of AAD technical support in designing and equipping the minicosms and Davis Station expeditioners in the summer of 2008 and 2009 for their support and assistance. The authors acknowledge the facilities, and the scientific and technical assistance of the Australian Microscopy and Microanalysis Facility at the Centre for Microscopy, Characterisation & Analysis, The University of Western Australia, a facility funded by the University, State and Federal Governments

LITERATURE CITED

Aberle N, Schulz KG, Stuhr A, Ludwig A, Riebesell U (2013) High tolerance of microzooplankton to ocean acidification in an Arctic coastal plankton community. Biogeosciences 10:1471–1481

Anonymous (2005) Inorganic non-metal constituents. In: Clesceri LS, Greenberg AE, Eaton AD (eds) Standard methods for the examination of water and wastewater, 21st edn. American Public Health Association, Washington, DC p 4–1/4–181

Azam F (1998) Microbial control of oceanic carbon flux: the plot thickens. Science 280:694–696

Barton A, Hales B, Waldbusser GG, Langdon C, Feely RA (2012) The Pacific oyster, *Crassostrea gigas*, shows negative correlation to naturally elevated carbon dioxide levels: implications for near-term ocean acidification effects. Limnol Oceanogr 57:698–710

Bothwell ML, Sherbot D, Pollock CM (1994) Ecosystem responses to solar ultraviolet-B radiation: influence of trophic level interactions. Science 265:97–100

Boyd CM, Heyraud M, Boyd CN (1984) Feeding of the Antarctic krill *Euphausia superba*. J Crustac Biol 4: 123–141

Bray JR, Curtis JT (1957) An ordination of upland forest communities of southern Wisconsin. Ecol Monogr 27: 325–349

Brévière E, Metzl N, Poisson A, Tilbrook B (2006) Changes of the oceanic CO_2 sink in the Eastern Indian sector of the Southern Ocean. Tellus 58:438–446

Brussaard CPD, Noordeloos AM, Witte H, Collenteur MCJ, Schulz K, Ludwig A, Riebesell U (2013) Arctic microbial community dynamics influenced by elevated CO_2 levels. Biogeosciences 10:719–731

Brzezinski MA (1985) The Si:C:N ratio of marine diatoms: interspecific variability and the effect of some environmental variables. J Phycol 21:347–357

Burkhardt S, Zondervan I, Riebesell U (1999) Effect of CO_2 concentration on C:N:P ratio in marine phytoplankton: a species comparison. Limnol Oceanogr 44:683–690

Burkhardt S, Amoroso G, Riebesell U, Sultemeyer D (2001) CO_2 and HCO_3^- uptake in marine diatoms acclimated to different CO_2 concentrations. Limnol Oceanogr 46: 1378–1391

Caldeira K, Wickett ME (2003) Oceanography: anthropogenic carbon and ocean pH. Nature 425:365

Caron DA, Hutchins DA (2013) The effects of changing climate on microzooplankton grazing and community structure: drivers, predictions and knowledge gaps. J Plankton Res 35:235–252

Chevin LM, Gallet R, Gomulkiewicz R, Holt RD, Fellous S (2013) Phenotypic plasticity in evolutionary rescue experiments. Phil Trans R Soc B 368:20120089

Clarke KR, Somerfield PJ, Gorley RN (2008) Testing of null hypotheses in exploratory community analyses: similarity profiles and biota-environment linkage. J Exp Mar Biol Ecol 366:56–69

Collins S, de Meaux J (2009) Adaptation to different rates of environmental change in *Chlamydomonas*. Evolution 63: 2952–2965

Cripps G, Lindeque P, Flynn KJ (2014) Have we been underestimating the effects of ocean acidification in zooplankton? Glob Change Biol 20:3377–3385

Danovaro R, Corinaldesi C, Dell'anno A, Fuhrman JA, Middelburg JJ, Noble RT, Suttle CA (2011) Marine viruses and global climate change. FEMS Microbiol Rev 35: 993–1034

Davidson AT (2006) Effects of ultraviolet radiation on microalgal growth, survival and production. In: Rao SDV (ed) Algal cultures, analogues of blooms and applications. Science Publishers, Enfield, NH, p 715–768

Delille D (2004) Abundance and function of bacteria in the Southern Ocean. Cell Mol Biol 50:543–551

Dickson A, Sabine C, Christian J (eds) (2007) Determination of total dissolved inorganic carbon in sea water. Guide to best practices for ocean CO_2 measurements. PICES Spec Publ 3. North Pacific Marine Science Organisation, Sidney

Ducklow HW, Steinberg DK, Buesseler KO (2001) Ocean carbon export and the biological pump. Oceanography (Wash DC) 14:50–58

Endres S, Galgani L, Riebesell U, Schulz KG, Engel A (2014) Stimulated bacterial growth under elevated pCO_2: results from an offshore mesocosm study. PLoS ONE 9: e99228

Engel A, Schulz KG, Riebesell U, Bellerby R, Delille B, Schartau M (2008) Effects of CO_2 on the particle distribu-

tion and phytoplankton abundance during a mesocosm bloom experiment (PeECE II). Biogeosciences 5:509–521

Engel A, Borchard C, Piontek J, Schulz K, Riebesell U, Bellerby R (2013) CO_2 increases ^{14}C-primary production in an Arctic plankton community. Biogeosciences 10: 1291–1308

Feely RA, Sabine CL, Hernandez-Ayon M, Ianson D, Hales B (2008) Evidence for upwelling of corrosive 'acidified' water onto the Continental Shelf. Science 320:1490–1492

Feng Y, Hare CE, Rose JM, Handy SM and others (2010) Interactive effects of iron, irradiance and CO_2 on Ross Sea phytoplankton. Deep-Sea Res I 57:368–383

Froneman PW, Perissinotto R (1996) Microzooplankton grazing and protozooplankton community structure in the South Atlantic and in the Atlantic sector of the Southern Ocean. Deep-Sea Res I 43:703–721

Gattuso JP, Lee K, Rost B, Schulz KG (2010) Approaches and tools to manipulate the carbonate chemistry. In: Riebesell U, Fabry VJ, Hansson L, Gattuso JP (eds) Guide to best practices for ocean acidification research and data reporting. Publications Office of the European Union, Luxembourg, p 41–52

Gattuso JP, Magan A, Billé R, Gheung WWL and others (2015) Contrasting future for ocean and society from different anthropogenic CO_2 emission scenarios. Science 349

Gehlen M, Gruber N, Gangsto R, Bopp L, Oschlies A (2011) Biogeochemical consequences of ocean acidification and feedbacks to the earth system. In: Gattuso JP, Hansson L (eds) Ocean acidification. Oxford University Press, Oxford, p 230–248

Gibson JAE, Trull TW (1999) Annual cycle of fCO_2 under sea ice and in open water in Prydz Bay, East Antarctica. Mar Chem 66:187–200

Giordano M, Beardall J, Raven JA (2005) CO_2 concentrating mechanisms in algae: mechanisms, environmental modulation and evolution. Annu Rev Plant Biol 56:99–131

Gong N, Wiens M, Schröder H, Mugnaioli E, Kolb U, Müller WEG (2010) Biosilicification of loricate choanoflagellate: organic composition of the nanotubular siliceous costal strips of *Stephanoeca diplocostata.* J Exp Biol 213:3575–3585

Gregg W, Ginoux P, Schopf PS, Casey NW (2003) Phytoplankton and iron: validation of a global three-dimensional ocean biogeochemical model. Deep-Sea Res II 50: 3143–3169

Grossart HP, Allgaier M, Passow U, Riebessell U (2006) Testing the effect of CO_2 concentration on the dynamics of marine heterotrophic bacterioplankton. Limnol Oceanogr 51:1–11

Guillard RRL, Kilham P (1977) The ec ology of marine planktonic diatoms. In: Werner D (ed) The biology of diatoms. University of California Press, Berkeley, CA, p 372–498

Hare CE, Leblanc K, DiTulio GR, Kudela RM and others (2007) Consequences of increased temperature and CO_2 for phytoplankton community structure in the Bering Sea. Mar Ecol Prog Ser 352:9–16

Harrison PH, Conway H, Holmes W, Davis D (1977) Marine diatoms grown in chemostats under silicate and ammonium limitation. III. Cellular chemical composition and morphology of *Chaetoceros debilis, Skeletonema costatum* and *Thalassiosira gravida.* Mar Biol 43:19–31

Havenhand JN, Schlegel P (2009) Near-future levels of ocean acidification do not affect sperm motility and fertilization kinetics in the oyster *Crassostrea gigas.* Biogeosciences 6:3009–3015

Hendriks IE, Duarte CM, Álvarez M (2010) Vulnerability of marine biodiversity to ocean acidification: a meta-analysis. Estuar Coast Shelf Sci 86:157–164

Hennon GMM, Ashworth J, Groussman RD, Berthiaume C, Morales R, Baliga NS, Orellana MV, Armbrust EV (2015) Diatom acclimation to elevated CO_2 via cAMP signalling and coordinated gene expression. Nat Clim Change 5: 761–766

Hinga KR (2002) Effects of pH on coastal marine phytoplankton. Mar Ecol Prog Ser 238:281–300

Hoffmann LJ, Breitbarth E, Boyd P, Hunter KA (2012) Influence of ocean warming and acidification on trace metal biogeochemistry. Mar Ecol Prog Ser 470:191–205

Hoppe CJM, Hassler CS, Payne CD, Tortell PD, Rost B, Trimborn S (2013) Iron limitation modulates ocean acidification effects on Southern Ocean phytoplankton communities. PLoS ONE 8:e79890

Hoppe CJM, Holtz LM, Trimborn S, Rost B (2015) Ocean acidification decreases the light use efficiency in an Antarctic diatom under dynamic but not constant light. New Phytol 207:159–171

Iglesias-Rodriguez MD, Halloran PR, Rickaby REM, Hall IR and others (2008) Phytoplankton calcification in a high CO_2 world. Science 320:336–340

IPCC (2014) Climate change 2014. Synthesis Report. Contribution of Working Groups I, II and III to the Fifth Assessment Report of the Intergovernmental Panel on Climate Change. IPCC, Geneva

Joint I, Doney SC, Karl DM (2011) Will ocean acidification affect marine microbes? ISME J 5:1–7

Kawaguchi S, Ichii T, Haganobu M (1999) Green krill, the indicator of micro-and nano-sized phytoplankton availability to krill. Polar Biol 22:133–136

Kawaguchi S, Ishida A, King R, Raymond B and others (2013) Risk maps for Antarctic krill under projected Southern Ocean acidification. Nat Clim Change 3: 843–847

Kim JM, Shin K, Lee K, Park BK (2008) *In situ* ecosystem-based carbon dioxide perturbation experiments: design and performance evaluation of a mesocosm facility. Limnol Oceanogr Methods 6:208–217

Kruskal JB (1964a) Multidimensional scaling by optimizing goodness-of-fit to a nonmetric hypothesis. Psychometrika 29:1–28

Kruskal JB (1964b) Nonmetric multidimensional scaling: a numerical method. Psychometrika 29:115–129

Kuipers BR, Witte HJ (1999) Grazing impact of microzooplankton on different size classes of algae in the North Sea in early spring and mid-summer. Mar Ecol Prog Ser 180:93–104

Larsen JB, Larsen A, Thyrhaug R, Bratbak G, Sandaa RA (2008) Responses of marine viral populations to a nutrient induced phytoplankton bloom at different pCO_2 levels. Biogeosciences 5:523–533

Legendre P, Anderson MJ (1999) Distance-based redundancy analysis: testing multispecies responses in multifactorial ecological experiments. Ecol Monogr 69:1–24

Legendre P, Oksanen J, Braak CJF (2011) Testing the significance of canonical axes in redundancy analysis. Methods Ecol Evol 2:269–277

Lewis E, Wallace DWR (1998) Program developed for CO_2 system calculations. ORNL/CDIAC-105. Carbon Dioxide Information Analysis Centre, Oak Ridge National Laboratory, US Dept of Energy, Oak Ridge, TN

Lohbeck KT, Riebesell U, Reusch TBH (2014) Gene expression changes in the coccolithophore *Emiliania huxleyi* after 500 generations of selection to ocean acidification. Proc R Soc B 281:20140003

Maas EW, Law CS, Hall JA, Pickmere S and others (2013) Effect of ocean acidification on bacterial abundance, activity and diversity in the Ross Sea, Antarctica. Aquat Microb Ecol 70:1–15

MacIsaac EA, Stockner JG (1993) Enumeration of picoplankton by autofluorescence microscopy. In: Kemp PF, Sherr BF, Sherr EB, Cole JJ (eds) Handbook of methods in aquatic microbial ecology. Lewis Publishers, Boca Raton, FL, p 187–197

Marchant HJ, Thomas DP (1983) Polylysine as an adhesive for the attachment of nanoplankton to substrates for electron microscopy. J Microsc 131:127–129

Marie D, Partensky F, Vaulot D, Brussaard C (1999) Enumeration of phytoplankton, bacteria, and viruses in marine samples. Curr Protoc Cytom, Suppl 10, 11.11.1, doi:10.1002/0471142956.cy111s10

McNeil BI, Sweeney C, Gibson JAE (2011) Natural seasonal variability of aragonite saturation state within two Antarctic coastal ocean sites. Antarct Sci 23:411–412

Miki T, Jacquet S (2008) Complex interaction in the microbial world: underexplored key links between viruses, bacteria and protozoan grazers in aquatic systems. Aquat Microb Ecol 51:195–208

Millero FJ, Woosley R, Ditrolio B, Waters J (2009) Effects of ocean acidification on the speciation of metals in seawater. Oceanography (Wash DC) 22:72–85

Morita M, Suwa R, Iguchi A, Nakamura M, Shimada K, Sakai K, Suzuki A (2010) Ocean acidification reduces sperm flagellar motility in broadcast spawning reef invertebrates. Zygote 18:103–107

Motegi C, Tanaka T, Piontek J, Brussaard CPD, Gattuso JP, Weinbauer MG (2013) Effect of CO_2 enrichment on bacterial metabolism in an Arctic fjord. Biogeosciences 10:3285–3296

Oksanen J, Blanchet FG, Kindt R, Legendre P and others (2015) vegan: Community Ecology Package. R package version 2.3-1. http://CRAN.R-project.org/package=vegan

Passow U, Carlson CA (2012) The biological pump in a high CO_2 world. Mar Ecol Prog Ser 470:249–271

Pearce I, Davidson AT, Bell EM, Wright S (2007) Seasonal changes in the concentration and metabolic activity of bacteria and viruses at an Antarctic coastal site. Aquat Microb Ecol 47:11–23

Pearce I, Davidson AT, Wright S, van den Enden R (2008) Seasonal changes in phytoplankton growth and microzooplankton grazing at an Antarctic coastal site. Aquat Microb Ecol 50:157–167

Peres-Neto PR, Jackson DA (2001) How well do multivariate data sets match? The advantages of a Procrusean superimposition approach over the Mantel test. Oecologia 129:169–178

Peres-Neto PR, Legendre P, Dray S, Borcard D (2006) Variation partitioning of species data matrices: estimation and comparison of fractions. Ecology 87:2614–2625

Piontek J, Lunau M, Händel N, Borchard C, Wurts M, Engel A (2010) Acidification increases microbial polysaccharide degradation in the ocean. Biogeosciences 7:1615–1624

Piontek J, Borchard C, Sperling M, Schulz KG, Riebesell U, Engel A (2013) Response of bacterioplankton activity in an Arctic fjord system to elevated pCO_2: results from a mesocosm perturbation study. Biogeosciences 10:297–314

Pomeroy LR, Williams J leB, Azam F, Hibbie JE (2007) The microbial loop. Oceanography (Wash DC) 20:28–33

Putland JN, Iverson RL (2007) Phytoplankton biomass in a subtropical estuary: distribution, size composition, and carbon:chlorophyll ratios. Estuar Coasts 30:878–885

R Core Team (2015). R: a language and environment for statistical computing. R Foundation for Statistical Computing, Vienna.

Redfield AC (1934) On the proportions of organic derivations in sea water and their relation to the composition of plankton. In: Daniel RJ (ed) James Johnstone memorial volume. University Press, Liverpool, p 177–192

Riebesell U, Schulz KG, Bellerby RGJ, Botros M and others (2007) Enhanced biological carbon consumption in a high CO_2 ocean. Nature 450:545–548

Roberts K, Granum E, Leegood RC, Raven JA (2007) Carbon acquisition by diatoms. Photosynth Res 93:79–88

Roden NP, Shadwick EH, Tilbrook B, Trull TT (2013) Annual cycle of carbonate chemistry and decadal change in coastal Prydz Bay, East Antarctica. Mar Chem 155:135–147

Rose JM, Caron DA, Sieracki ME, Poulton N (2004) Counting heterotrophic nanoplanktonic protists in cultures and aquatic communities by flow cytometry. Aquat Microb Ecol 34:263–277

Rose JM, Feng Y, Gobler CJ, Gutierrez R, Hare CE, Leblanc K, Hutchins DA (2009) Effects of increased pCO_2 and temperature on the North Atlantic spring bloom. II. Microzooplankton abundance and grazing. Mar Ecol Prog Ser 388:27–40

Rost B, Riebesell U, Burkhardt S, Sultemeyer D (2003) Carbon acquisition of bloom-forming marine phytoplankton. Limnol Oceanogr 48:55–67

Rost B, Zondervan I, Wolf-Gladrow D (2008) Sensitivity of phytoplankton to future changes in ocean carbonate chemistry: current knowledge, contradictions and research directions. Mar Ecol Prog Ser 373:227–237

Roy AS, Gibbons SM, Schunck H, Owens S and others (2013) Ocean acidification shows negligible impacts on high-latitude bacterial community structure in coastal pelagic mesocosms. Biogeosciences 10:555–566

Saba GK, Schofield O, Torres JJ, Ombres EH, Steinberg DK (2012) Increased feeding and nutrient excretion of adult Antarctic krill, *Euphausia superba*, exposed to enhanced carbon dioxide (CO_2). PLoS ONE 7:e52224

Schaum E, Rost B, Millar AJ, Collins S (2013) Variation in plastic responses of a globally distributed picoplankton species to ocean acidification. Nat Clim Change 3:298–302

Schulz KG, Riebesell U, Bellerby RGJ, Biswas H and others (2008) Build-up and decline of organic matter during PeECE III. Biogeosciences 5:707–718

Schulz KG, Bellerby RGJ, Brussaard CPD, Bündenbender J and others (2013) Temporal biomass dynamics of an Arctic bloom in response to increased levels of atmospheric carbon dioxide. Biogeosciences 10:161–180

Scott FJ, Marchant HJ (2005) (eds) Antarctic marine protists. Australian Biological Resources Study, Canberra and Australian Antarctic Division, Hobart

Shi D, Xu Y, Morel FMM (2009) Effects of pH and pCO_2 control method on medium chemistry and phytoplankton growth. Biogeosciences 6:1199–1207

Shi D, Xu Y, Hopkinson BM, Morel FMM (2010) Effect of ocean acidification on iron availability to marine phytoplankton. Science 327:676–679

Smetacek V (2008) Are declining krill stock a result of global warming or of the decimation of the whales? In: Duarte CM (ed) Impacts of global warming on polar systems. Fundación BBVA, Bilbao, p 47–83

Sperling M, Piontek J, Gerdts G, Wichels A and others (2013) Effect of elevated CO_2 on the dynamics of particle-attached and free-living bacterioplankton communities in an Arctic fjord. Biogeosciences 10:181–191

Suffrian K, Simonelli P, Nejstgaard JC, Putzeys S, Carotenuto Y, Anita AN (2008) Microzooplankton grazing and phytoplankton growth in marine minicosms with increased CO_2 levels. Biogeosciences 5:1145–1156

Takahashi T, Sutherland SC, Sweeney C, Poisson A and others (2002) Global sea-air CO_2 flux based on climatological surface ocean pCO_2, and seasonal biological and temperature effects. Deep-Sea Res II 49:1601–1622

Thomson PG, Davidson AT, Cadman N (2008) Temporal changes in effects of ambient UV radiation on natural communities of Antarctic marine protists. Aquat Microb Ecol 52:131–147

Thomson PG, Davidson AT, van den Enden R, Pearce I, Seuront L, Paterson JS, Williams G (2010) Distribution and abundance of marine microbes in the Southern Ocean between 30 and 80°E longitude. Deep-Sea Res II 57:815–827

Thomson PG, Davidson AT, Maher L (2016) Increasing pCO_2 changes community composition of pico- and nano-sized protists and prokaryotes at a coastal Antarctic site. Mar Ecol Prog Ser (in press)

Tomas CR (ed) (1997) Identifying marine phytoplankton. Academic Press, San Diego, CA

Torstensson A, Heldblom M, Andersson J, Andersson MX, Wulff A (2013) Synergism between elevated pCO_2 and temperature on the Antarctic sea ice diatom *Nitzschia lecointei.* Biogeosciences 10:6391–6401

Tortell PD, DiTullio GR, Sigman DM, Morel FMM (2002) CO_2 effects on taxonomic composition and nutrient utilization in an Equatorial Pacific phytoplankton assemblage. Mar Ecol Prog Ser 236:37–43

Tortell PD, Payne CD, Li Y, Trimborn S and others (2008) CO_2 response of Southern Ocean phytoplankton. Geophys Res Lett 35:L04605, doi:10.1029/2007GL032583

Trimborn S, Brenneis T, Sweet E, Rost B (2013) Sensitivity of Antarctic phytoplankton to ocean acidification: growth, carbon acquisition and species interactions. Limnol Oceanogr 58:997–1007

Vila-Costa M, Gasol JM, Sharma S, Moran MA (2012) Community analysis of high- and low-nucleic acid-containing bacteria in NW Mediterranean coastal waters using 16SrDNA pyrosequencing. Environ Microbiol 14: 1390–1402

Wright SW, van den Enden RL, Pearce I, Davidson AT, Scott FJ (2010) Phytoplankton community structure and stocks in the Southern Ocean (30–80°E) determined by CHEMTAX analysis of HPLC pigment signatures. Deep-Sea Res II 57:758–778

Yamada N, Suzumura M (2010) Effects of seawater acidification on hydrolytic enzyme activities. J Oceanogr 66: 233–241

Zhang R, Xia X, Lau SCK, Motegi C, Weinbauer MG, Jiao N (2013) Response of bacterioplankton community structure to an artificial gradient of pCO_2 in the Arctic Ocean. Biogeosciences 10:3679–3689

Editorial responsibility: Steven Lohrenz, New Bedford, Massachusetts, USA

Submitted: October 21, 2014; Accepted: April 23, 2016
Proofs received from author(s): June 14, 2016